Supporting Information

Redox of Dual Radical Intermediates in a Methylene-linked Covalent Triazine Framework for High Performance Lithium Ion Batteries

*Zhiqiang Wang [a], Shuai Gu [a,b], Lujie Cao [a], Long Kong [a], Zhenyu Wang [a], Ning Qin [a,b], Muqing Li [a], Wen Luo [a], Jingjing Chen [a], Sisi Wu [a], Guiyu Liu [a], Huimin Yuan [a], Yunfei Bai [a], Kaili Zhang [b], and Zhouguang Lu [a]**

a. Department of Materials Science and Engineering, Guangdong-Hong Kong-Macao Joint Laboratory for Photonic-Thermal-Electrical Energy Materials and Devices, Southern University of Science and Technology, Shenzhen 518055 Guangdong, P. R. China.

b. Department of Mechanical Engineering, City University of Hong Kong, 83 Tat Chee Avenue, Kowloon, Hong Kong, P.R. China.

Corresponding Author's email address

* luzg@sustech.edu.cn

Table of Contents

S1 Experimental Procedures

Chemicals

Materials All chemicals were purchased from commercial suppliers (Extension, Sigma-Aldrich and Alfa Aesar chemical company) and used without further purification, unless stated otherwise. Anhydrous chloroform ($CHCl_3$) was distilled from P_2O_5 under a nitrogen atmosphere according to the reported procedures. Trifluoromethanesulfonic acid (97%) was purchased from Adamas-beta, p-Xylylene Dicyanide (99%) was purchased from Aladdin. All other reagents were obtained from commercial suppliers and used as received unless otherwise noted.

Characterization

FT-IR spectra data were collected with a PerkinElmer FT-IR spectrometer in the 400-4000 cm^{-1} region (KBr pressed disks). Thermo-gravimetric analysis (TGA) was performed at a heating rate of 10 K/min under N_2 atmosphere using a PerkinElmer TGA 7. Powder X-ray diffraction (PXRD) data were collected over the 2θ range 2°~ 80° on a CPS120 Inel diffractometer equipped with Ni-filtered Cu K*α* radiation (40 kV, 25 mA) at room temperature with a scan speed of 2° min^{-1}. Scanning electron microscopy (SEM) experiments were performed on Zeiss Merlin and TESCAM MIRA3 scanning electron microscope. Electron paramagnetic resonance (EPR) spectra are recorded on a Bruker EMXplus-10/12 spectrometer under room temperature. The microwave frequency was 9.8 GHz and the modulation amplitude microwave power were about 1 mW. And the spectra were obtained by one scan. After charging and discharging to the specified voltage, the electrode sheets were washed with DMC (dimethyl carbonate) in glove box, then dried, stripped, and used for EPR sample preparation. Raman spectra were collected on a Renishaw inVia Raman Spectrometer (wavelength: 633 nm and power: 0.5 mW) (copper nanoparticle as a conductive agent). NEWARE battery cycler (CT-4008T-5V10mA-164, Shenzhen, China) testing systems were used for galvanostatic charge/discharge experiments. Cyclic voltammetry (CV) analyses were performed with a Bio-Logic VMP3 work station. X-ray Photon Spectroscopy (XPS, Perkin-Elmer PHI 550) with Al K Alpha as the X-ray source. C1s XPS spectra of CTF-p electrode at different states: as-made, discharge to 4.3 V, discharge to 2.8 V and discharge to 1.0 V. X-ray Photon Spectroscopy (XPS, Perkin-Elmer PHI 550) with Al K Alpha as the X-ray source. Electrodes for XPS testing contain 80 wt% active material, 10 wt% CNT, and 10 wt% PVDF. Samples were prepared by disassembling cells in the Ar-filled glovebox, washing the electrodes with dimethyl carbonate (DMC) for three times, and drying the electrodes in vacuum. Then the samples were obtained by scratching the electrodes for XPS measurements.

Sample preparation

To evidence the electrochemical performance of the CTF-p polymers as anodecathode materials in Li-ion battery, the working electrodes were prepared by mixing the CTF-p, acetylene black, carbon nanotubes and polytetrafluoro ethylene (PTFE) binder in a mass ratio of 3:3:3:1.

Synthesis of CTF-p

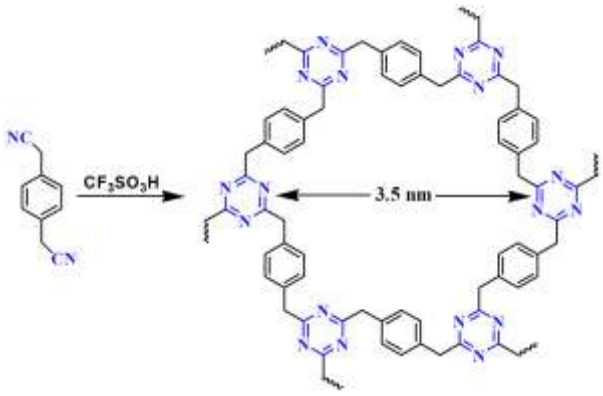

Figure S1. Schematic of the CTF-p preparation.

Trifluoromethanesulfonic acid (0.6 mL, 6.8 mmol) and anhydrous $CHCl_3$ (10 mL) were added to a 100 mL pre-dried three-necked round bottom flask under nitrogen atmosphere. The mixture was stirred at 0 °C for 0.5 h, and the monomer p-Xylylene Dicyanide (200 mg, 0.42 mmol) was dissolved in anhydrous $CHCl_3$ (20 mL) and added dropwise into the prepared mixture over 30 min. The mixture was stirred for 2 h under 0 °C, and then the temperature was raised to 100 ºC and stirred for another 48 h. The yellow CTF-p semi-crystalline with shining appearance were obtained then quenching with ethanol (5 mL). The obtained solid was filtered and washed with water, dichloromethane, acetone dimethyl carbonate and ethanol (10 mL×3), successively. The solid was dried in vacuum at 70 °C for 24 h to give a light brown powder (156 mg, yield: 78%).

Caculation

DFT calculations were performed with B3LYP/6-31G(d,p) method via Gaussian 16, Revision A.03 software package to investigate the electrochemical properties of CTF-p structure. Structures were fully optimized for each molecule using 6-31G(d,p) basis set which was rationalized in the study of methylene-linked CTF and confirmed as true local minimum by vibrational frequency analyses.[2] All calculated results of molecular electrostatic potential (MESP) and Electron spin densities were performed with Multiwfn 3.6 programs.[3] All visualization of MESP plots are carried out by Multiwfn software. The convergence criterion of the total energy is 10-5 Hartree.
For this part we set the key word "opt" in Gaussian input file and therefore the convergence criterions used for calculation are the corresponding ones, including:
Requested convergence on RMS density matrix=1.00D-08 within 128 cycles.
Requested convergence on MAX density matrix=1.00D-06.
Requested convergence on energy=1.00D-06.

Results and Discussion

S2. FT-IR spectra of CTF-p and monomer

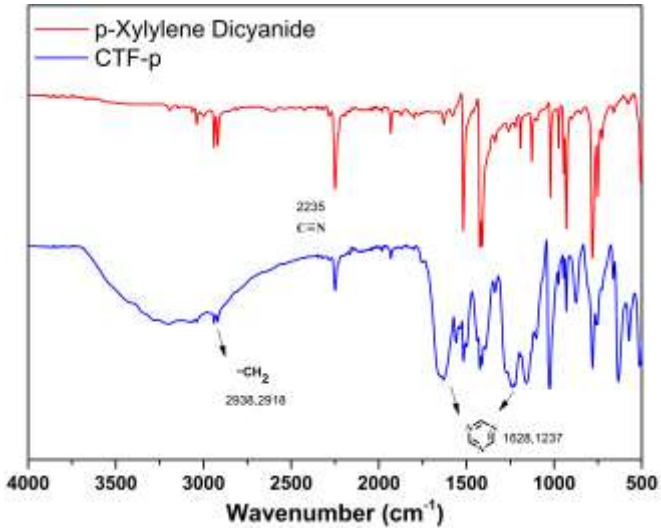

Figure S2. FT-IR spectrums of CTF-p and monomer.

S3. PXRD spectra of CTF-p and monomer

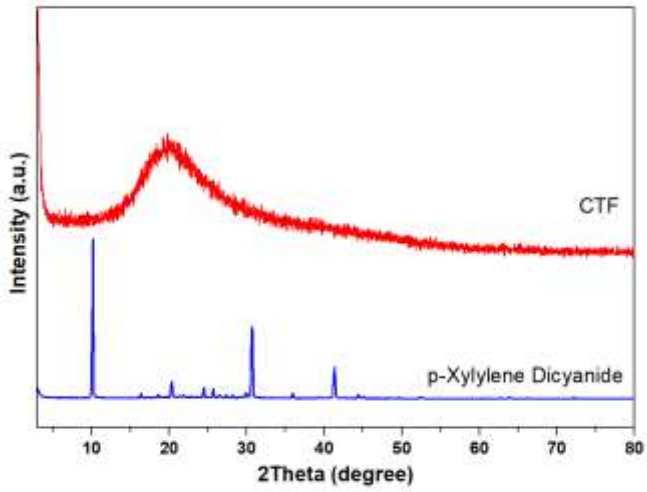

Figure S3. P-XRD spectrums of CTF-p and monomer.

S4. TGA curve of CTF-p

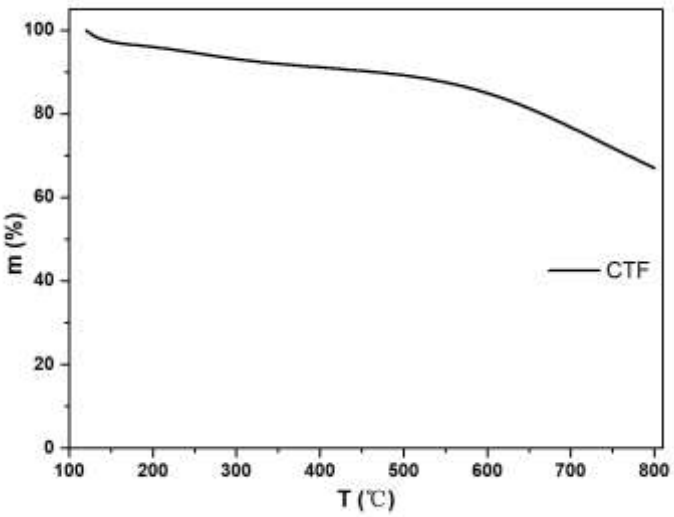

Figure S4. TGA curve of CTF-p.

S5. SEM images

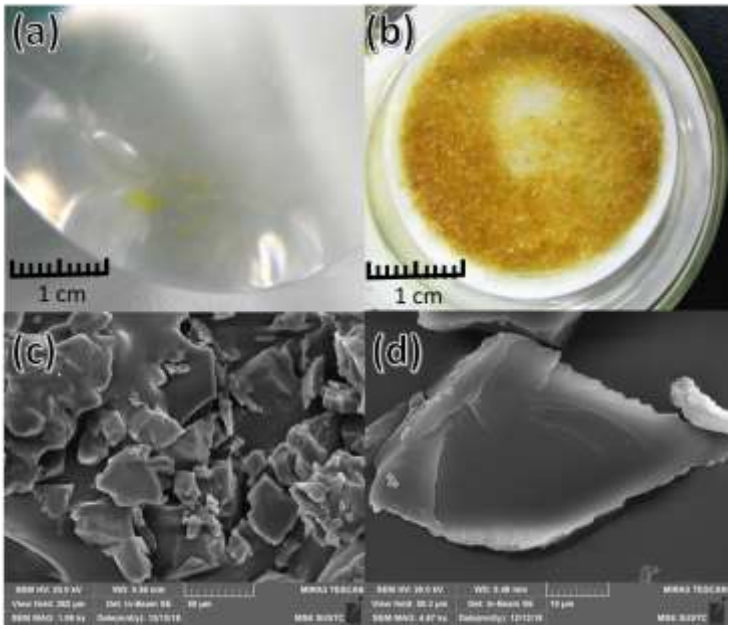

Figure S5. (a) The photograph of CTFs in DMF. (b) The photograph of CTFs after filter. and (c, d) Scanning electron microscopy (SEM) for the CTFs.

S6. Galvanostatic charge and discharge profiles at a current density of 100 mA g−1

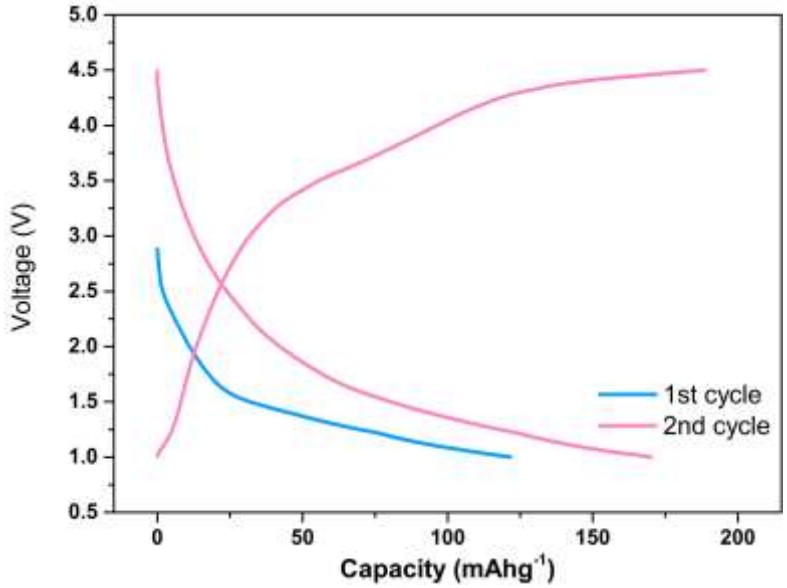

Figure S6. Galvanostatic charge and discharge profiles at a current density of 100 mA g^{-1}.

S7. The Nyquist plots images

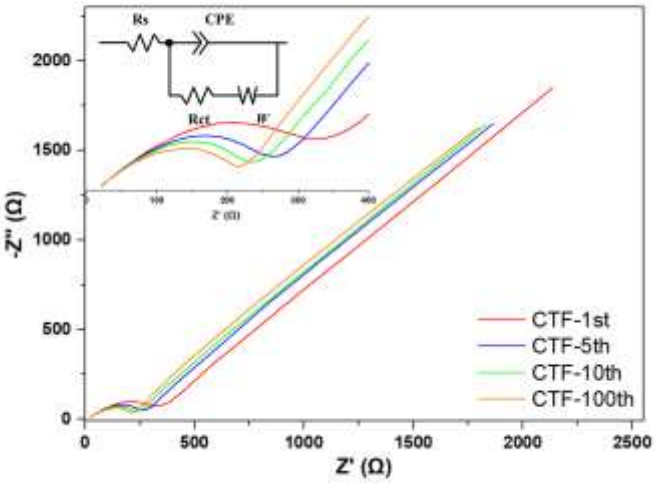

Figure S7. The Nyquist plots of the CTF-p cells (after cycling 1st, 5th, 10th and 100th) do not show anomalously high resistances suggesting that the electrode conductivity does not limit capacity.

The CTF materials show wider semicircles indicating larger resistances in the cathode electrode before cycling. The narrower semicircles in the Nyquist plots after cycling indicate a decrease in the charge transfer resistance of the electrodes. Relatively, the lower charge transfer resistance (Rct) of CTF-p materials (332 Ω decrease to 212 Ω) may cause by Faraday reactions occurring on SEI after cycling for 100 th, these electrodes produce protective materials and allow good transmission during the closer contact between battery membrane and anode plate. Besides, the lithium ion diffusion coefficient (DLi^+) of CTF-p is calculated to be 3.35×10^{-16} cm^2 s^{-1}, which is lower than that of bulk CTF-1 (1.07×10^{-13} cm^2 s^{-1}).

S8. The long-term cycling of CTF-p for 1 C

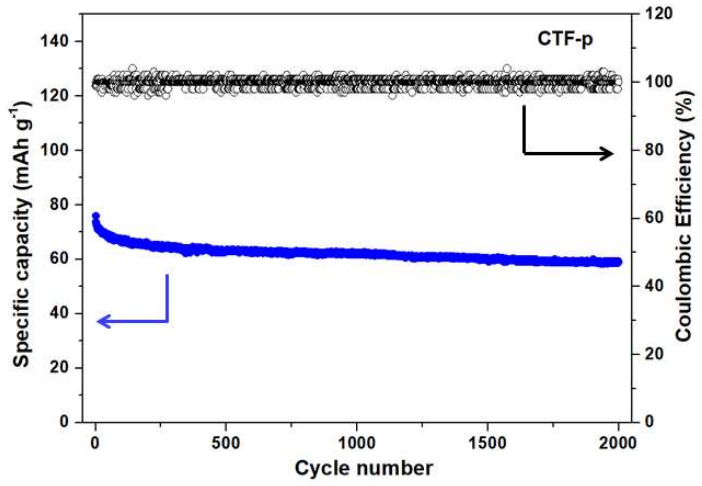

Figure S8. The long-term cycling experiments for 2000 cycles at a current density of 1 C.

S9. EPR spectra of pristine CTF-p

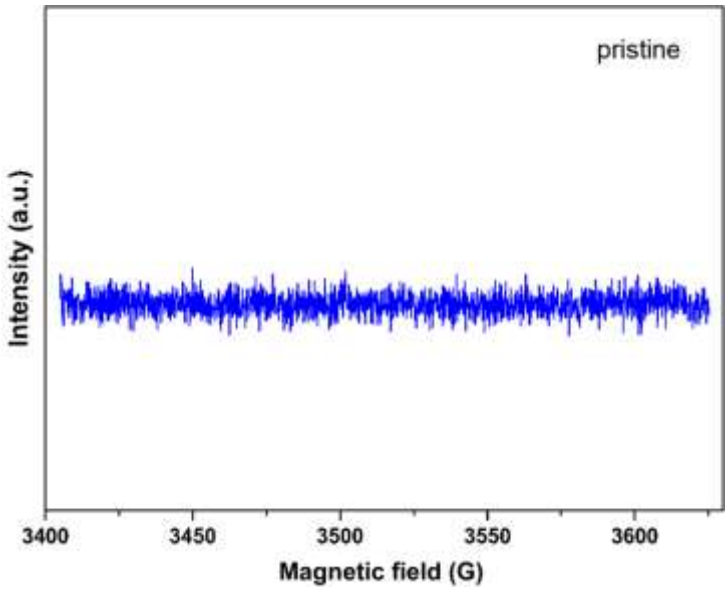

Figure S9. EPR spectra of pristine CTF-p.

S10. EPR spectra of PVDF

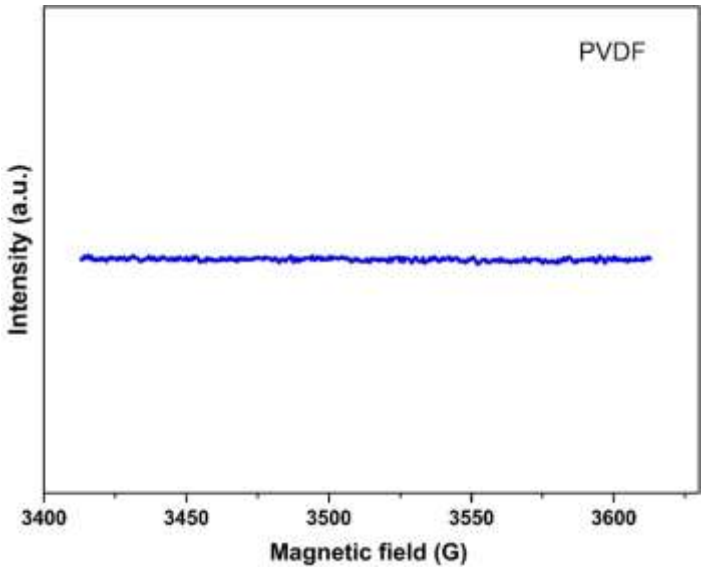

Figure S10. EPR spectra of PVDF.

S11. The ex-situ electron paramagnetic resonance (EPR) spectra during charging and discharging of the CTFs

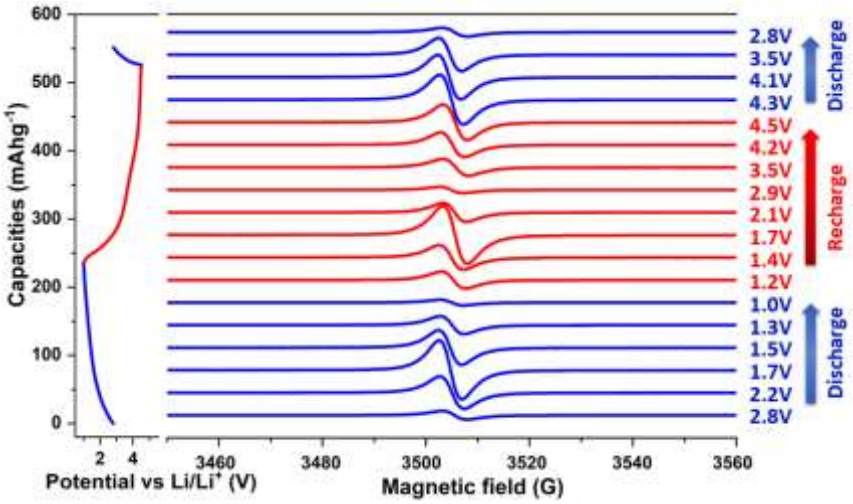

Figure S11. the ex-situ electron paramagnetic resonance (EPR) spectra during charging and discharging of the CTFs.Consistent with the reported works, the unpaired electron could be delocalized and distributed on the triazine ring and its attached substituents.[4]

S12. EPR spectra of the electrode being discharge to 1.7V after 20 and 50 cycles.

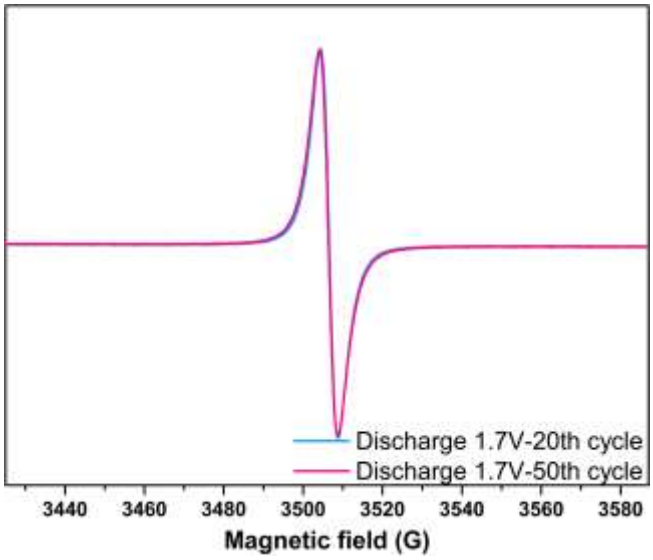

Figure S12. EPR spectra of the electrode being discharge to 1.7V after 20 and 50 cycles.

S13. The atomic coordinates of CTF-p.

Table S1. The atomic coordinates of CTF-p.

Center Number	Element	Coordinates(Angstroms) X	Y	Z	Center Number	Element	Coordinates(Angstroms) X	Y	Z
1	C	2.715	-7.228	-0.609	82	C	0.112	8.172	-2.114
2	C	1.511	-7.083	-1.263	83	C	7.207	4.313	-2.22
3	C	0.252	-7.478	-0.703	84	C	6.662	5.503	-2.65
4	N	-2.197	-9.226	-0.543	85	C	5.344	5.924	-2.261
5	C	-2.161	-8.025	-1.28	86	H	8.209	4.039	-2.534
6	C	-0.936	-7.363	-1.467	87	H	7.249	6.162	-3.287
7	H	3.643	-7.046	-1.146	88	N	2.464	7.884	-2.317
8	H	1.514	-6.711	-2.287	89	C	3.72	7.762	-1.698
9	C	-7.981	-4.928	-2.956	90	C	4.854	7.237	-2.508
10	C	-7.354	-6.155	-3.101	91	H	2.309	7.711	2.409
11	C	-6.117	-6.449	-2.455	92	N	3.873	7.911	-0.353
12	H	-8.971	-4.785	-3.384	93	C	2.803	8.222	0.369
13	H	-7.869	-6.958	-3.624	94	C	2.934	8.423	1.849
14	N	-3.29	-7.605	-1.947	95	H	2.603	9.431	2.14
15	C	-4.442	-8.253	-1.71	96	C	4.575	4.946	-1.535
16	C	-5.663	-7.816	-2.336	97	C	5.124	3.764	-1.101
17	H	-4.15	-10.892	1.316	98	C	6.498	3.432	-1.332
18	N	-4.552	-9.319	-0.83	99	H	3.548	5.185	-1.272
19	C	-3.379	-9.787	-0.347	100	H	4.52	3.082	-0.506
20	C	-3.454	-11.041	0.482	101	N	9.256	3.306	-0.29
21	C	0.313	-7.986	0.686	102	C	8.466	2.17	-0.333
22	C	1.536	-8.144	1.33	103	C	7.084	2.324	-0.674
23	C	2.781	-7.79	0.752	104	H	-7.07	-3.153	3.473
24	H	-0.608	-8.073	1.256	105	N	-8.759	-1.55	2.073
25	H	1.537	-8.505	2.358	106	C	-8.244	-2.758	1.726
26	N	5.088	-5.975	0.871	107	C	-7.845	-3.647	2.873
27	C	5.194	-7.23	1.347	108	H	-7.462	-4.613	2.531
28	C	4.015	-8.026	1.439	109	C	8.458	-3.163	-0.586
29	C	8.93	-1.679	1.755	110	C	9.909	-1.603	0.694

30	C	7.709	-2.327	1.596	111	N	8.906	0.948	-0.011
31	C	7.359	-3.018	0.358	112	N	6.376	-7.764	1.83
32	H	9.122	-1.125	2.671	113	C	10.535	3.113	0.101
33	H	6.99	-2.337	2.412	114	C	7.424	-6.922	1.848
34	N	7.427	-5.669	1.41	115	H	10.963	5.045	0.945
35	C	6.228	-5.176	0.847	116	N	11.077	1.943	0.394
36	C	6.182	-3.917	0.317	117	C	11.396	4.342	0.223
37	H	-2.475	-11.315	0.886	118	C	9.679	-2.525	-0.41
38	C	-5.468	-5.338	-1.827	119	H	8.306	-3.808	-1.449
39	C	-6.094	-4.087	-1.74	120	H	10.448	-2.631	-1.174
40	C	-7.397	-3.864	-2.22	121	C	10.257	0.81	0.303
41	H	-4.52	-5.485	-1.313	122	C	10.797	-0.435	0.585
42	H	-5.589	-3.282	-1.212	123	H	11.452	4.859	-0.743
43	N	-8.057	-3.186	0.492	124	H	9.32	-6.677	2.85
44	C	-8.412	-2.313	-0.568	125	C	8.724	-7.47	2.384
45	C	-8.143	-2.646	-1.863	126	H	9.317	-7.907	1.57
46	H	-5.743	3.857	4	127	H	-3.845	-11.871	-0.117
47	N	-4.78	6.758	2.608	128	H	-8.703	-3.816	3.533
48	C	-5.539	5.641	2.782	129	H	-4.126	4.604	4.021
49	C	-5.203	4.809	3.991	130	H	3.971	8.294	2.172
50	C	-8.558	1.941	-0.278	131	H	12.405	4.077	0.546
51	C	-8.048	3.209	-0.59	132	H	8.547	-8.257	3.125
52	C	-8.446	4.369	0.091	133	H	4.034	-8.826	2.18
53	H	-8.105	1.073	-0.753	134	H	5.237	-3.588	-0.122
54	H	-7.272	3.287	-1.348	135	H	11.881	-0.552	0.483
55	N	-6.507	5.245	1.982	136	H	6.413	1.565	-0.275
56	C	-6.805	6.052	0.853	137	H	5.556	7.947	-2.96
57	C	-7.726	5.654	-0.063	138	H	0.04	7.659	-3.071
58	C	-1.168	9.59	-0.479	139	H	-4.074	9.308	2.212
59	C	-2.27	9.717	0.337	140	H	-7.886	6.28	-0.938
60	C	-3.393	8.826	0.236	141	H	-10.396	0.495	2.297
61	H	-0.322	10.259	-0.352	142	H	-8.55	-2.011	-2.647
62	H	-2.281	10.479	1.113	143	H	-6.375	-8.597	-2.598
63	N	-6.12	7.267	0.696	144	H	-0.9	-6.692	-2.327
64	C	-5.138	7.536	1.539	145	Li	-6.203	-8.408	-0.136
65	C	-4.32	8.739	1.315	146	Li	-0.324	-9.698	-0.353
66	H	-5.453	5.364	4.904	147	Li	-4.102	-6.612	-3.384
67	C	-9.461	4.205	1.066	148	Li	6.428	-9.725	2.104
68	C	-9.951	2.955	1.418	149	Li	3.241	-5.552	0.633
69	C	-9.472	1.754	0.802	150	Li	8.81	-4.293	1.346
70	H	-9.817	5.085	1.598	151	Li	11.959	1.136	1.949
71	H	-10.681	2.872	2.22	152	Li	7.996	-0.797	-0.102
72	N	-9.101	-1.138	-0.263	153	Li	8.097	4.946	-0.119
73	C	-9.218	-0.793	1.022	154	Li	3.191	7.143	-3.873
74	C	-9.829	0.475	1.368	155	Li	-0.121	8.057	0.919
75	C	-3.41	7.982	-0.924	156	Li	5.675	7.13	-0.004
76	C	-2.312	7.871	-1.747	157	Li	-2.846	7.181	2.65
77	C	-1.091	8.564	-1.48	158	Li	-7.433	3.46	2.089
78	H	-4.27	7.344	-1.099	159	Li	-6.212	9.114	0.082
79	H	-2.334	7.156	-2.567	160	Li	-10.291	0.286	-0.757
80	N	1.525	8.351	-0.162	161	Li	-7.445	-5.027	-0.039
81	C	1.413	8.172	-1.519	162	Li	-8.153	0.118	2.992

S14. The electrochemical property comparison among the organic materials as anodes for sodium-ion batteries.

Table S2. The electrochemical property comparison among the organic materials as anodes for sodium-ion batteries.

Sample	Capacity	Ref
CTF-p	**247 mAh/g at 100 mA/g**	**This work**
ACTF-1	140 mAh/g at 100 mA/g	[5]
CTF-400-1	23 mAh/g at 100 mA/g	[6]

References

[1] Karmakar A.; A. Kumar.; Chaudhari A. K.; Samanta P.; Desai A. V.; Krishna R.; Ghosh S. K. Bimodal Functionality in a Porous Covalent Triazine Framework by Rational Integration of an Electron-Rich and ‐Deficient Pore Surface. *Chem. Eur. J.* **2016**, *22*, 4931-4937. DOI: 10.1002/chem.201600109

[2] Liang Y.; Zhang P.; Chen J. Function-oriented design of conjugated carbonyl compound electrodes for high energy lithium batteries *Chem. Sci. J.* **2013**, *4*, 1330-1337. DOI: 10.1039/C3SC22093A

[3] Shi R.; Liu L.; Lu Y.; Wang C.; Li Y.; Li L.; Yan Z.; Chen J. Nitrogen-rich covalent organic frameworks with multiple carbonyls for high-performance sodium batteries *Nature Comm*. **2020**, *11*, 178. DOI: 10.1038/s41467-019-13739-5

[4] Catalin, M.; Adil, M.; Miche,l.; Marius, A.; Nigel, G. R.; Rodolphe, C.; Narcis, A. C_3 symmetric tris(phosphonate)-1,3,5-triazine ligand: homopolymetallic complexes and its radical anion. *New J. Chem.* **2010**, *34*, 2319–2327.

[5] Sakaushi, K.; Nickerl, G.; Nickerl, G.; Gemming, T.; Zhou, H, S.; Kaskel, S.; Eckert, J. Aromatic Porous-honeycomb Electrodes for a Sodium-organic Energy Storage Device. *Nat. Commun.* **2013**, *4*, 1485. DOI: 10.1038/ncomms2481

[6] See, K. A.; Hug, S.; Schwinghammer, K.; Lumley, M. A.; Zheng, Y. H.; Nolt, J. M.; Stucky, G. D.; Wudl, F.; Lotsch, B. V.; Seshadri, R. Lithium Charge Storage Mechanisms of Cross-Linked Triazine Networks and Their Porous Carbon Derivatives. *Chem. Mater.* **2015**, *27*, 3821-3829. DOI: acs.chemmater.5b00772